

RESEARCH

Open Access



# Effect of pyrolytic temperature on the adsorption of Pb(II) from synthetic wastewater onto bamboo chopstick biochar: a conventional vs. microwave-assisted pyrolysis approach

Thembeke Mabaso<sup>1</sup>, Shang-Lien Lo<sup>1,2,3\*</sup>  and Pei-Te Chiueh<sup>1,2,3</sup>

## Abstract

This study investigated the effects of different pyrolytic temperatures on Pb(II) adsorption from synthetic wastewater using waste bamboo chopsticks (BCs) produced via conventional and microwave-assisted pyrolysis. Eleven biochars were prepared and characterized using Brunauer–Emmett–Teller analysis, elemental analysis, scanning electron microscopy, and Fourier transform infrared spectroscopy. Thereafter, the selected biochars were further analyzed through batch adsorption studies. The influence of adsorbent dose, initial Pb(II) concentration, and contact time on the removal of Pb(II) from synthetic wastewater was studied. For the adsorbent dose, good removal efficiencies and adsorption capacities were observed at an adsorbent dose of  $2 \text{ g L}^{-1}$  and at an initial concentration of  $50 \text{ mg L}^{-1}$ . For the initial Pb(II) concentration, high adsorption capacities and removal efficiencies were observed at  $50 \text{ mg L}^{-1}$  for concentrations ranging from 5 to  $100 \text{ mg L}^{-1}$ . The contact time reached equilibrium within 24 h, where BC 450 W had the highest removal efficiency of 99.9%. Furthermore, the Langmuir isotherm model best represented the adsorption of Pb(II) onto biochar, with the highest  $q_m$  of  $81 \text{ mg g}^{-1}$  at  $R^2 = 0.978$ . Pseudo-second-order kinetics provided the best overall fit for the adsorption kinetics of the biochars, with  $R^2 = 1.00$  for BC 450 W and BC 700 °C. Among the many chemisorption processes identified in previous studies, surface complexation has been identified as a possible adsorption mechanism for Pb(II) on the biochars produced. BC biochar could be a sustainable means for remediating polluted mine water and managing waste.

**Keywords** Biochar, Microwave-assisted pyrolysis, Conventional pyrolysis, Bamboo chopsticks, Pb(II) adsorption, Adsorption kinetics, Adsorption mechanisms

## 1 Introduction

The mining process entails the extraction of precious metals and other geologically important materials from the earth which has been economically vital in the growth of civilization, providing resources for areas such as energy generation, construction, and manufacturing in its broadness. However, shortfalls have also been associated with mining primarily in the release of

\*Correspondence:  
Shang-Lien Lo  
sll@ntu.edu.tw

<sup>1</sup> Graduate Institute of Environmental Engineering, National Taiwan University, Taipei 10617, Taiwan

<sup>2</sup> Water Innovation, Low Carbon and Environmental Sustainability Research Center, National Taiwan University, Taipei 10617, Taiwan

<sup>3</sup> Science and Technology Research Institute for DE-Carbonization (STRIDE-C), National Taiwan University, Taipei 10617, Taiwan



© The Author(s) 2024. **Open Access** This article is licensed under a Creative Commons Attribution 4.0 International License, which permits use, sharing, adaptation, distribution and reproduction in any medium or format, as long as you give appropriate credit to the original author(s) and the source, provide a link to the Creative Commons licence, and indicate if changes were made. The images or other third party material in this article are included in the article's Creative Commons licence, unless indicated otherwise in a credit line to the material. If material is not included in the article's Creative Commons licence and your intended use is not permitted by statutory regulation or exceeds the permitted use, you will need to obtain permission directly from the copyright holder. To view a copy of this licence, visit <http://creativecommons.org/licenses/by/4.0/>.

heavy metals as byproducts, which pose as major environmental and health hazards.

Heavy metal byproducts of mining that are commonly identified as toxic and are of concern include arsenic (As), cadmium (Cd), lead (Pb), and mercury (Hg). Among these metals, lead (Pb) stands out for its recyclability and widespread use in various industries, including automotive, paint, pipe, and petrol [1]. However, lead exposure can severely impact multiple body systems, causing neurological and behavioural issues, kidney damage, cancer and anaemia [2, 3].

The presence of dissolved metals in water bodies harms aquatic life, damages waterways, and alters landscapes. Pb(II)-contaminated soils lack essential nutrients for plant growth, hindering revegetation efforts and causing long-term environmental damage. Without treatment, Pb(II) can pollute water sources, endangering ecosystems and potentially impacting human health [4]. Heavy metals that are byproducts of mining, including Pb(II), negatively affect plant functions, leading to bioaccumulation in both plants and animals, ultimately increasing species mortality rates [4, 5]. In regions facing water scarcity, implementing practical methods and circular economy principles could help develop effective solutions for removing Pb(II) and other byproducts of mining, contributing to sustainable waste management practices. In previous studies, conventional methods have been used to find effective means of remediating the Pb(II)-contaminated water. These methods include membrane filtration, reverse osmosis, ion exchange, precipitation, peroxide oxidation, coagulation, and adsorption [6–9]. Among these, adsorption technology is favoured because it is commercially beneficial, adaptable, simple, and effective for eliminating heavy metals [7].

Adsorption is affected by various factors, such as temperature, composition, type of adsorbates and adsorbents, and occurrence of contaminants. In addition, operational conditions such as pH, pollutant concentration, contact time, adsorbent dosage, and adsorbent particle size contribute to overall adsorption once the characteristics of the adsorbent are determined [9–11]. Adsorption methods are widely used to purify wastewater from both organic and inorganic toxins without generating hazardous byproducts [10]. Various porous materials have been investigated in removing impurities from wastewater by choosing these adsorbents owing to their porous structure and significant surface area. These materials include activated carbon, mesoporous carbon, nanometal oxides, metal–organic frameworks, carbon nanotubes, biochar, and zeolites [12–15]. Among these materials, biochar was of particular importance in this study.

Biochar is an important substance produced through pyrolysis that serves many purposes, including the remediation of contaminated water, atmospheric carbon capture, and soil conditioning for fertility [15, 16]. Biochar is derived from a variety of materials, including manure; spoil from the paper and cellulose industries; agricultural waste such as coconut shells, bamboo, and sugarcane bagasse; and solid organic wastes, such as sewage sludge [17, 18]. Chopsticks, particularly disposable bamboo chopsticks (BC), are widely used in Southeast Asian cutleries. Owing to their convenience and sanitary advantages, nonreusable chopsticks add considerably to environmental pollution by accumulating in landfills after single use, posing a challenge for waste management in many Asian countries [19]. Restoring disposable chopsticks as biochar feedstock perfectly aligns with circular economy principles through eliminating waste thus pollution, greatly contributing to environmental sustainability through synergistic relations of societies and the environment [2], particularly when utilized as biochar for environmental purposes [18, 19].

Many studies have explored the use of biochar produced via conventional pyrolysis (CP) for the removal of heavy metals, particularly Pb(II), from aqueous solutions. Few studies have been conducted on biochar produced via microwave-assisted pyrolysis (MAP). However, Godwin et al. [20] reported that MAP can further modify the shape of biochar, thus increasing its surface area and making it more suitable for removing heavy metals and other contaminants.

MAP biochar offers an advantage due to its fast-heating rates which helps in activating the biochar through the development of a microporous structure, oxygen containing functional groups at its surface and improvement of catalytic activities [9, 19]. Since bamboo chopsticks are known to contain a lot of lignin, cellulose and hemicellulose; MAP is able to produce biochar that has been irradiated from within, further enabling the biochar produced to have high surface area and large pore volume for effective pollutant removal [11, 16].

With approximately 80 billion chopstick pairs produced in China and distributed worldwide per annum, their rate in use and disposal therefore are yet to be recorded. However, the contribution of this waste to overall pollution can be reduced to limit environmental problems like air pollution, water contamination, and soil diseases. Transferring it into biochar material is a promising way to ensure this. Although this material has already been presented in several studies where BC had been carbonized into carbon-based energy, for CO<sub>2</sub> capture, and bio-oil accumulation [12, 21, 22]. However, studies on BC biochar were in their infancy when this study was conducted where previous studies mainly

focused on characterization, soil application and p-nitrophenol removal [17, 19, 23]. This work investigates the adsorption properties and adsorption mechanisms of Pb(II) on BC biochars produced using conventional horizontal pyrolysis and MAP, comparing their characterizations and effectiveness in adsorbing Pb(II).

In this study, novelty is noted in the use of disposable BC as feedstock for biochar produced through MAP and compared to BC that is produced by conventional means at different thermal conditions to compare its effectiveness based on its physicochemical differences in the removal of Pb(II) typically found in contaminated wastewater.

Therefore, this study aimed to evaluate the effect of various temperatures on the production of BC biochars generated through CP and MAP for the treatment of synthetic wastewater containing Pb(II). The objectives of this research include the following key points: (1) to synthesize and characterize pristine biochars produced using CP and MAP methods at various temperatures or powers; (2) to assess and compare how the manufacturing temperature or power influence the capacity of different pristine biochars to adsorb Pb(II) in synthetic wastewater by studying the physicochemical characteristics, adsorption kinetics and isotherms; and (3) to propose the adsorption mechanisms of pristine biochar after Pb(II) adsorption to understand the methods involved in Pb(II) removal.

## 2 Materials and methods

### 2.1 Materials

Waste BCs were collected from the institution's cafeteria and dormitories at National Taiwan University. The raw materials were cleaned and oven-dried for 12 h. Furthermore, the materials were pulverized using a grinder, sieved through a number 50 mesh sieve (0.297 mm), stored in plastic containers and placed in a desiccator prior to biochar production. Lead nitrate ( $\text{Pb}(\text{NO}_3)_2$ ) was acquired from Sigma Aldrich (United Kingdom) and used without further refinement to prepare a 1000 mg  $\text{L}^{-1}$  stock solution of single-element synthetic wastewater, which was further diluted to the preferred concentrations during analyses.

### 2.2 Biomass composition

Using the ASTM D1762-84 standard, BC biomass was analyzed to evaluate its physical composition through proximate analysis. These physical components include the moisture, volatile matter, and ash content of the biomass before it is subjected to pyrolysis. Two different elemental analyzers were used to determine the elemental compositions of the raw biomass and biochar throughout the study. The first elemental analyzer used was an

Elementar UNI cube from Germany, which provided the ultimate analysis of the sample, specifically measuring the composition of carbon (C), nitrogen (N), and hydrogen (H). Another elemental analyzer (Elementar Vario EL Cube, Germany) was primarily used for oxygen analysis.

### 2.3 Biochar preparation

#### 2.3.1 CP

Pulverized BC were placed in ceramic boats and pyrolyzed in a horizontal tube furnace (Thermo Fischer Scientific Lindberg/Blue M, USA). The tube furnace was then heated at a rate of  $10\text{ }^\circ\text{C min}^{-1}$  from room temperature to the desired temperature (300, 400, 500, 600, and  $700\text{ }^\circ\text{C}$ ) under a  $100\text{ mL min}^{-1}$  nitrogen gas purge, where the biomass was pyrolyzed for 60 min. After the experiment, the resulting biochar was collected, cooled, washed with deionized water, dried at  $70\text{ }^\circ\text{C}$  for 24 h, and stored in a desiccator until further analysis. The different bamboo biochar samples were labelled BC  $300\text{ }^\circ\text{C}$ , BC  $400\text{ }^\circ\text{C}$ , BC  $500\text{ }^\circ\text{C}$ , BC  $600\text{ }^\circ\text{C}$ , and BC  $700\text{ }^\circ\text{C}$ , indicating the temperatures used for their production. The experiments were conducted in triplicates to ensure reproducibility of results.

#### 2.3.2 MAP

Finely ground waste BC, weighing approximately 20 g, were placed in quartz glass crucible subjected to MAP using a single-mode microwave oven operating at a frequency of 2.45 GHz and a maximum power output of 2000 W [19]. A thermocouple sensor was placed at the base of the quartz crucible to monitor the temperatures of the biomass samples at different microwave power levels. To ensure oxygen-free conditions, nitrogen gas was introduced continuously into the system at a flow rate of  $100\text{ mL min}^{-1}$ . Once a stable inert environment was achieved, the microwave power was activated and set to a predetermined level for 20 min.

The synthesized biochar was then allowed to cool in a desiccator and washed with deionized water. The biochar was then dried in an oven at  $70\text{ }^\circ\text{C}$  for 24 h and stored in a desiccator before application. MAP was conducted across a range of microwave powers varying from 200 to 450 W: BC 200 W, BC 250 W, BC 300 W, BC 350 W, BC 400 W, and BC 450 W. The experiments were conducted in triplicates to ensure reproducibility of results.

### 2.4 Characterization of bamboo chopstick biochar

Various methods have been used to characterize biochar. These include proximate analysis of the biomass, scanning electron microscopy (SEM), elemental composition analysis, Brunauer–Emmett–Teller (BET) analysis, and spectroscopy. Proximate analysis of the bamboo chopsticks biomass was conducted using the ASTM Standard

Test Method D1762–84 to determine the proximate and ultimate analyses through calculations using the obtained data, which yielded moisture, volatile matter, fixed carbon, and ash results. Fourier transform infrared (FTIR) spectroscopy was used to study the surface functional groups of the biochars produced at various pyrolysis temperatures, and analyses were performed using a Perkin Elmer IS10 spectrometer (Perkin Elmer, USA) comprising of a KBr pellet containing between 1–2% of the biochar produced, a wavelength range from 4000 to 400  $\text{cm}^{-1}$ , with 8 scans per analysis. FTIR spectroscopy was used to analyze the changes in the functional groups of the biochars before and after Pb(II) adsorption. The surface morphologies of the biochar samples were examined by SEM (JEOL JSM-7600F, Japan). Furthermore, textural features and pore structures, including the BET-specific surface area, pore size and total volume of the biochars, were studied using the automated surface area and porosity system ASAP 2420 (Micromeritics, USA) where degassing of approximately 0.15 g of sample occurred for 12 h and results were obtained after conducting micropore analyses. Elemental Analyses were conducted using Elementar UNI cube (Germany), which measured the composition of carbon (C), nitrogen (N), and hydrogen (H), and Elementar Vario EL Cube (Germany), which was primarily designed for oxygen analysis.

### 2.5 Adsorption isotherm and kinetics studies

Batch adsorption experiments were conducted to evaluate the Pb(II) removal efficiency and adsorption capacities of the selected biochars, namely, BC 200 W, BC 450 W, BC 500 °C, and BC 700 °C. Aqueous solutions with various concentrations of  $\text{Pb}(\text{NO}_3)_2$  were prepared as heavy metal sources. The biochar samples (0.05 g) were mixed with 25 mL of Pb(II) solution in 50 mL conical centrifuge tubes, shaken in a reciprocal oscillating bath (Yih Der BT-350, Taiwan) at 180 rpm for 24 h, and allowed to settle. The solutions were filtered through a 0.45  $\mu\text{m}$  syringe filter and analyzed for Pb concentrations using inductively coupled plasma–optical emission spectrometry (Perkin Elmer Optima 8300 DV, USA). All batch adsorption experiments were carried out at room temperature in triplicate. All experiments were conducted at a pH of 5 using 0.1 M NaOH/0.1 M HCl. The effects of the adsorbent dose, initial Pb(II) concentration, and contact time were investigated to evaluate the overall influence of the biochar. The removal efficiencies and adsorption capacities were evaluated using equations (Eqs. (S1) and (S2)) in the Supplementary Materials.

For the adsorption kinetic studies, 0.05 g of BC at various temperatures was added to 25 mL of a 50  $\text{mg L}^{-1}$  solution of Pb(II) to evaluate the adsorption process as a function of time (0, 60, 120, 360, 720, and 1440 min) at

25 °C for 24 h. The study of the adsorption isotherms was also performed by adding 0.05 g of biochar to 50 mL of a Pb(II) solution at different concentrations (5, 10, 20, 50, 100  $\text{mg L}^{-1}$ ) in 50 mL conical flasks, stirred constantly at 180 rpm, 25 °C for 24 h. The points  $t=0$ ,  $C_e=0$  and  $q_{t=0}$  were added to adsorption and kinetic data as required to model the initial adsorption stage in the respective analyses.

To effectively analyze the isotherm and kinetics data, common models for isotherms, including the Langmuir and Freundlich models, and traditional models for kinetics, such as the pseudo-first-order (PFO) and pseudo-second-order (PSO) models, were used.

### 2.6 Statistical analyses

All the data were statistically analyzed and plotted using Microsoft Excel 2019 and OriginPro 2024 (Originlab Corporation, 2024). All the tables were designed using Microsoft Word 2019. The t-test was performed on OriginPro 2024 to statistically observe the significance ( $p \leq 0.05$ ) of removal efficiencies and adsorption capacities in the effect of adsorbent doses and initial Pb(II) concentrations.

## 3 Results and discussion

### 3.1 Characterization of the biochars produced

#### 3.1.1 Proximate analysis

Proximate analysis of the raw BC produced moisture, volatile matter, fixed carbon, and ash contents that were 8.8, 71.7, 18.6, and 0.7%, respectively. The moisture content obtained was double that reported by Xu et al. [17], but it was still less than 10%, which indicates that the biomass was pyrolyzed uniformly during the analysis [15], whereas the ash content was 0.7%, which was less than that reported by Xu et al. [17]. Low ash and moisture contents signify favorable feedstocks where binding active sites are available and accessible upon application [16]. However, the volatile matter and fixed carbon results for bamboo chopstick biomass are similar to those reported by Xu et al. [17], and these results indicate the high reactivity and applicability of the feedstock when it is pyrolyzed. The results obtained are depicted in Table 1.

#### 3.1.2 Elemental analysis

The results of the ultimate analysis of the biochar samples produced using different pyrolysis methods and thermal conditions are shown in Table 2, where BC is indicative of BC biochar. When the temperature was increased from 300 °C to 700 °C for CP (BC 300 °C to BC 700 °C), the C content of the biochar increased from 68–87%, whereas for microwave pyrolysis (BC 200 W to BC 450 W), it was observed that with an increase in power, there was an increase until BC 400 W and a decrease at BC 450 W to

**Table 1** Proximate and ultimate analysis of pulverized bamboo chopsticks

Proximate Analysis	Percentage (wt.%)
Moisture	8.89 ± 0.00
Volatile matter	71.76 ± 0.02
Fixed carbon	18.65 ± 0.04
Ash	0.71 ± 0.02
Ultimate Analysis	Percentage (wt.%)
C	46.05 ± 0.01
H	6.51 ± 0.04
N	0.16 ± 0.01
O	47.40 ± 0.13

Remark: Average data are depicted with standard deviations

76.3%. The C content increased due to the formation of a more condensed carbon structure through the polymerization reaction and reduction of (-OH) surface functional groups from all the biochars via dehydration [17, 23]. In contrast, the O content decreases with increasing pyrolysis temperature and microwave power. The O content in both the MAP and CP biochars was drastically reduced in the respective biochar samples because of the dissociation of weaker bonds and greater CO and CO<sub>2</sub> losses in the early stages of pyrolysis [24]. Both methods produced biochars with a negligible mass fraction of nitrogen; however, the nitrogen content increased when the pyrolysis temperature increased from 300 to 500 °C owing to its resistance to heating and not being easily volatilized. This observed trend agreed with the results obtained by [22], in which the H content gradually decreased with increasing temperature.

As indicated in Table 2, the H/C and O/C ratios decreased with increasing microwave power for MAP and with increasing temperature for CP. The H/C atomic ratio decreased from 0.61 for BC 200 W to 0.31 for BC 450 W, whereas for CP, the ratio decreased from 0.71 for BC 300 °C to 0.26 for BC 700 °C. This indicated that the unsaturated carbons in the sugars and carbohydrates of the biomass that were difficult to hydrolyze and decompose were transformed into relatively stable C with higher aromaticity and saturation in the biochar, especially with increasing temperature and power [19]. According to Fahmi et al. [25], the H/C ratio can serve as a reliable gauge of biochar aromaticity and stability, with increased stability being linked to lower H/C ratios.

Furthermore, the O/C ratio is a significant indicator of biochar stability, where the typical ratio range is between 0.2 and 0.6. Biochars with values closer to 0.6 have lower stability, and those with values lower than 0.2 show even greater stability [23]. This was noted for the biochars produced using both pyrolytic methods, where the O/C ratio decreased for all biochars with increasing thermal conditions. The ultimate analysis yielded results that were comparable to those reported in the literature [11, 17].

**3.1.3 Surface area and pore analysis**

To further characterize the biochar produced, BET tests were performed, and the results of the MAP biochar were compared with those of CP BC (Table 3). The development of pores within BC biochar during CP and MAP is anticipated. The BC biochars produced using conventional pyrolysis had lower BET surface areas between 18 and 234 m<sup>2</sup> g<sup>-1</sup> and pore sizes within a smaller range of 3.7–5.8 nm. In the context of MAP, the BET surface

**Table 2** Ultimate analysis of bamboo chopstick biochar produced at different temperatures and via different methods

Sample	Biochar Yield (%)	Ultimate Analysis (%)				Atomic Ratios	
		C	H	N	O	H/C	O/C
Microwave Assisted Pyrolysis							
BC 200 W	23.30 ± 2.82	73.59 ± 0.22	3.79 ± 0.19	0.37 ± 0.03	21.57 ± 0.19	0.61 ± 0.03	0.21 ± 0.05
BC 250 W	16.75 ± 0.63	80.24 ± 0.09	2.97 ± 0.04	0.40 ± 0.00	15.85 ± 0.24	0.44 ± 0.01	0.15 ± 0.00
BC 300 W	13.25 ± 2.19	81.38 ± 0.26	2.60 ± 0.02	0.44 ± 0.01	15.10 ± 0.10	0.38 ± 0.00	0.14 ± 0.00
BC 350 W	12.97 ± 3.02	82.85 ± 0.11	2.40 ± 0.00	0.47 ± 0.01	14.57 ± 0.25	0.34 ± 0.00	0.13 ± 0.00
BC 400 W	7.85 ± 1.48	82.92 ± 0.16	2.23 ± 0.28	0.43 ± 0.00	14.51 ± 0.23	0.32 ± 0.04	0.13 ± 0.00
BC 450 W	5.25 ± 0.07	76.33 ± 0.19	2.01 ± 0.01	0.42 ± 0.00	14.79 ± 0.25	0.31 ± 0.00	0.15 ± 0.00
Conventional Pyrolysis							
BC 300°C	36.00 ± 2.54	68.47 ± 0.18	4.10 ± 0.01	0.36 ± 0.01	25.67 ± 0.06	0.72 ± 0.00	0.28 ± 0.00
BC 400°C	26.25 ± 0.64	76.31 ± 0.04	3.65 ± 0.00	0.37 ± 0.01	17.36 ± 0.20	0.57 ± 0.00	0.17 ± 0.00
BC 500°C	23.39 ± 2.18	83.96 ± 0.10	3.16 ± 0.00	0.40 ± 0.00	9.47 ± 0.01	0.45 ± 0.00	0.08 ± 0.00
BC 600°C	21.16 ± 0.19	81.34 ± 0.08	2.47 ± 0.01	0.36 ± 0.00	12.19 ± 0.19	0.36 ± 0.00	0.11 ± 0.00
BC 700°C	19.56 ± 0.03	87.28 ± 0.28	1.89 ± 0.03	0.38 ± 0.00	9.37 ± 0.05	0.26 ± 0.00	0.08 ± 0.00

Remark: Average data are depicted with standard deviations

**Table 3** BET specific area and pore volume analysis of biochar produced via microwave-assisted and conventional pyrolysis

Pyrolysis Method	Adsorbent	$S_{\text{BET}}$ ( $\text{m}^2 \text{g}^{-1}$ )	$V_{\text{T}}$ ( $\text{cm}^3 \text{g}^{-1}$ )	Average Pore Size (nm)
MAP	BC 200 W	166	0.058	10.62
	BC 250 W	342	0.008	4.30
	BC 300 W	288	0.093	5.85
	BC 350 W	268	0.092	5.08
	BC 400 W	270	0.070	4.34
	BC 450 W	414	0.120	3.70
CP	BC 300 °C	19	0.004	5.85
	BC 400 °C	60	0.014	4.46
	BC 500 °C	81	0.026	4.75
	BC 600 °C	173	0.052	4.93
	BC 700 °C	234	0.031	3.75

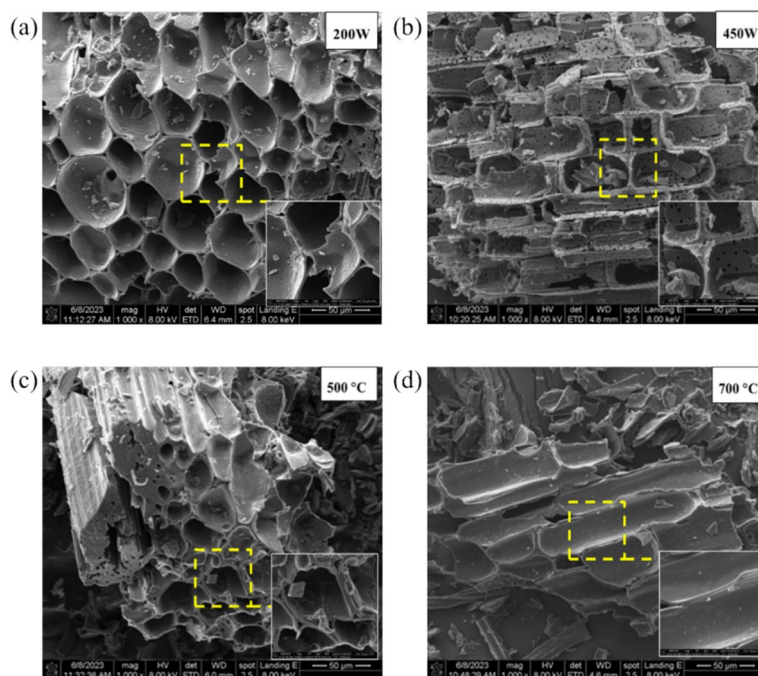
areas ranged from 165 to 414  $\text{m}^2 \text{g}^{-1}$ , and the pore sizes varied between 3.7 and 10.6 nm (Table 3). The biochar generated at 450 W exhibited the highest BET surface area of 414  $\text{m}^2 \text{g}^{-1}$  and the smallest pore size of 3.7 nm. The biochar produced by MAP exhibited smaller pores, resulting in a greater surface area than that generated by CP (Table 3). These observations are consistent with the findings of Islam et al. [26] and Mari Selvam and Balasubramanian [27], where biochar derived from microwave

pyrolysis facilitated the thermal degradation of condensable hydrocarbons trapped within biochar pores, leading to the production of gaseous byproducts. This phenomenon contributed to the increase in biochar porosity and surface area. Additionally, BC containing lignin, cellulose, and hemicellulose undergo uneven degradation during thermal conversion, impacting biochar surface characteristics, specifically pore size and distribution [22]. Notably, all the BC biochars displayed mesoporous features, with pore sizes ranging from 3.7 to 10.6 nm.

### 3.1.4 SEM surface analysis

The SEM micrographs in Fig. 1 show that the biochars produced primarily displayed honeycomb and hollow tubular structures, suggesting a wooden origin [17]. As the pyrolysis temperature increased, more pores appeared on the walls of the hollow tubes, primarily for BC 450 W and BC 700 °C. This phenomenon results from the thermal degradation of hemicellulose, cellulose, and lignin during pyrolysis, leading to the release of volatiles and the formation of pores [11, 17, 26, 27].

The biochars derived from BC biomass pyrolyzed at various temperatures exhibited relatively smooth surfaces, with some exhibiting visible mesoporous pores, which is consistent with the average pore size results presented in Table 3. For the MAP, BC 200 W, BC 300 W, BC 350 W, and BC 450 W exhibited distinct pore formations that varied and became more distinct with increasing

**Fig. 1** Micrographs depicting MAP biochar (a) BC 200 W and (b) BC 450 W and CP biochar (c) BC 500 °C and (d) BC 700 °C

power and temperature, as noted in Fig. 1a and b and Fig. S1.

From the SEM images, it is evident that the BC biochars prepared via CP at BC 400 °C (Fig. S2), BC 500 °C, and BC 700 °C (Figs. 1c and d) exhibit honeycomb-like pore structures with well-defined pores. Specifically, the biochar prepared at 500 °C displayed precisely defined pores with the emergence of new small pores, similar to the findings obtained by Xu et al. [17]. The biochars produced through MAP were highly porous and displayed a rougher surface with increasing power, and biochars produced through CP produced notably smoother surfaces (see Fig. 1).

### 3.1.5 FTIR spectroscopy of the biochar before batch adsorption studies

The physicochemical properties of biochar, which are determined by its functional groups, govern its ability to remove Pb(II). Figure 2 shows the FTIR spectra of BC produced using different pyrolysis methods, namely, MAP and CP. The FTIR spectra of the microwave-pyrolyzed biochar displays distinct peaks. The strong and broad bands at approximately 3438  $\text{cm}^{-1}$  were notable for BC 200 W and BC 450 W for microwave pyrolysis (Fig. 3a), while a similar band at approximately 3415  $\text{cm}^{-1}$  was prominent for BC 500 °C and BC 700 °C for CP (Fig. 3b). This band corresponds to the stretching vibrations of O–H [17, 28].

As the pyrolysis temperature increased during CP, the sharp O–H band was not as prominent as when the spectra were observed at lower temperatures. This is due to the pyrolysis of the components that make up the biochar, leading to the loss of functional groups due

to the volatility of the products produced, such as  $\text{CO}_2$  [17]. However, in microwave pyrolysis, the O–H band decreased from 200 to 350 W, reappeared at 400 W, and persisted at 450 W. This suggests a reduced water content with increased temperature for CP and increased hydrogen bonding sites with elevated power for microwave pyrolysis, which is indicative of the presence of cellulose and hemicelluloses [17, 28].

The C–H stretching vibrations of alcohol and phenol structures (2900  $\text{cm}^{-1}$ ), the C=O stretching vibration of carboxylic acids (1700  $\text{cm}^{-1}$ ), and the strong band at approximately 1600  $\text{cm}^{-1}$  due to aromatic ring group compounds are present in both MAP and CP biochar [11]. In addition, the absorbance peaks at 1100–1120  $\text{cm}^{-1}$  were attributed to C–O stretching vibrations [17]. These peaks gradually decreased with biochar produced at increased temperature ranging from 300 to 700 °C. For microwave pyrolysis, the C–H stretching vibrations at approximately 2900  $\text{cm}^{-1}$  decreased at powers of 250–300 W and reappeared from 400 to 450 W. Biochar produced at lower temperatures through CP between 300 and 400 °C shows diverse organic characteristics, including aliphatic structures, and is composed of more C–H and C=C functional groups [28].

## 3.2 Evaluation of batch adsorption

### 3.2.1 Effect of the adsorbent dose

Increasing the adsorbent dose (2–10  $\text{g L}^{-1}$ ) yielded varied results for biochar produced by CP and MAP. At a dosage of 2  $\text{g L}^{-1}$ , the removal efficiency trend was BC 450 W > BC 700 °C > BC 500 °C > BC 200 W, with the highest removal efficiency of 99.7% for BC 450 W. At a dosage of 4  $\text{g L}^{-1}$ , the removal efficiency decreased in the order

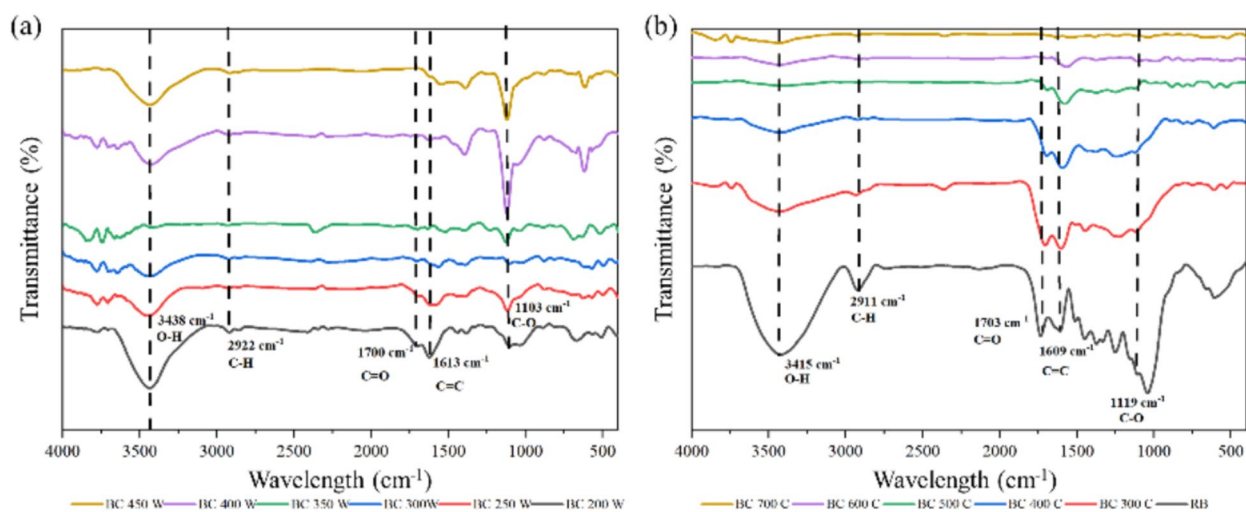


**Fig. 2** FTIR spectra of the bamboo chopstick biochar produced with a) MAP and b) CP

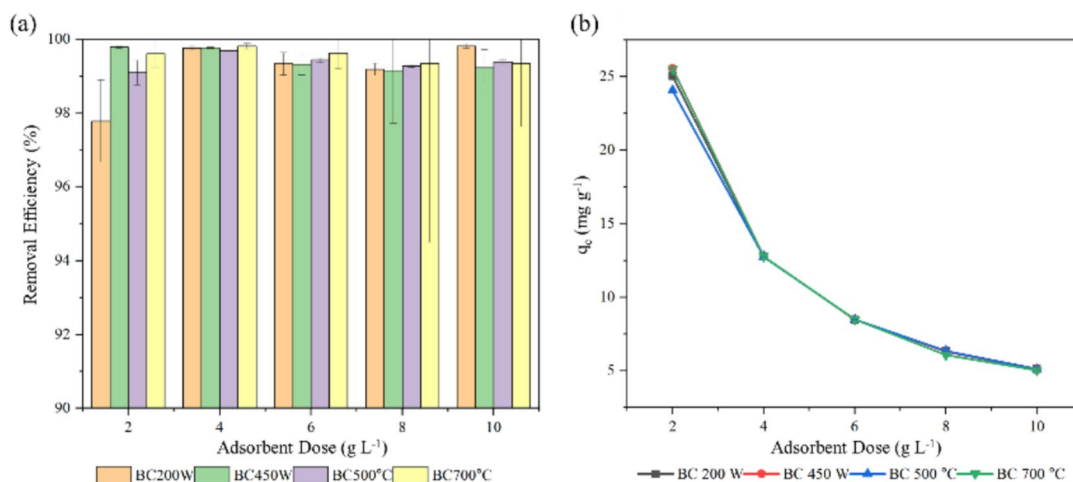


**Fig. 3** Graphs depicting (a) the removal efficiency of Pb(II) and (b) the adsorption capacity of the biochar at different adsorption capacities of the selected adsorbents produced using different pyrolysis methods

BC 700 °C > BC 450 W > BC 200 W > BC 500 °C, with the highest removal efficiency of 99.8% for BC 700 °C. At 6 and 8 g L<sup>-1</sup>, BC at 700 °C maintained the highest biochar activity, followed by BC at 500 °C, 200 W, and 450 W, with BC removal efficiencies ranging between 99.3% and 99.6% at 700 °C. At 10 g L<sup>-1</sup>, BC at 200 W surpassed biochar activity, followed by BC at 500 °C, BC at 700 °C, and BC at 450 W; achieving the highest removal efficiency of 99.8% (see Fig. 3). With these results, statistical analyses were conducted to observe the effects of adsorbent dose on the biochar studied, finding that p-values for adsorbent dose in relation to removal efficiencies were < 0.0001. This indicated great significance due to the

difference in the data range of the factors observed and not necessarily the impact of the results (Table S1).

Furthermore, the results indicate that biochars produced at higher temperatures or power (700 °C and 450 W) demonstrated the highest removal efficiencies, with adsorption capacities of 25.6 and 25.5 mg g<sup>-1</sup> for BC 450 W and BC 700 °C, respectively, at 2 g L<sup>-1</sup> (Fig. 4). Overall, the results showed over 80% removal of Pb(II) across the investigated adsorbents at different dosages, and the adsorption capacities were notably greater at 24–25 mg g<sup>-1</sup> at 2 g L<sup>-1</sup> than at higher dosages after 24 h of contact, which correlates with Eq. (S2) in the supplementary materials, as the adsorption capacity

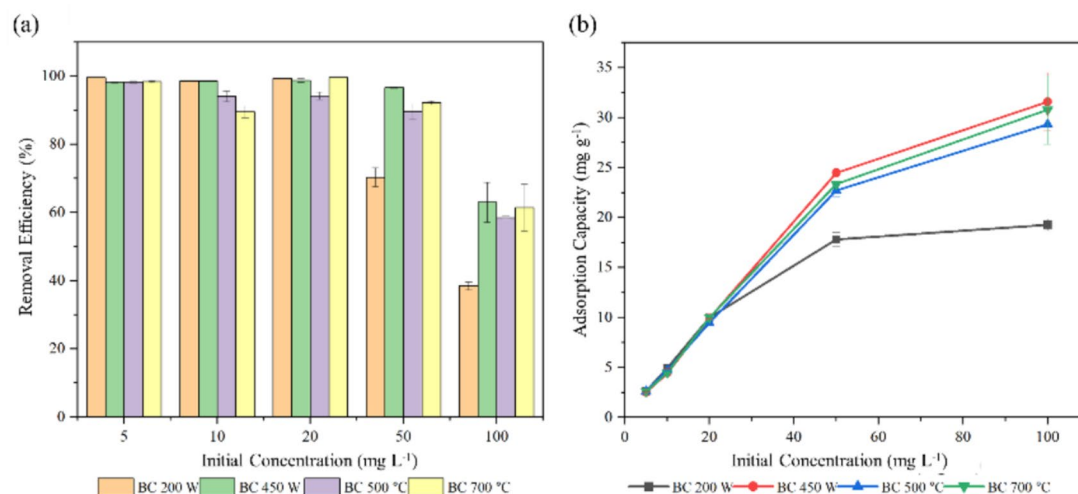


**Fig. 4** Graphs depicting (a) the removal efficiency of Pb(II) and (b) the adsorption capacity of the biochar at different initial Pb concentrations for the 4 selected biochars produced using different pyrolysis methods

decreases with increasing mass [29]. Similar findings were observed in a study conducted by Chen et al. [30] where lower adsorbent doses were preferred as adsorption capacities observed were greater. This observation guides further studies conducted, where an adsorbent dose of  $2 \text{ g L}^{-1}$  will be used for all adsorption isotherm and kinetic studies.

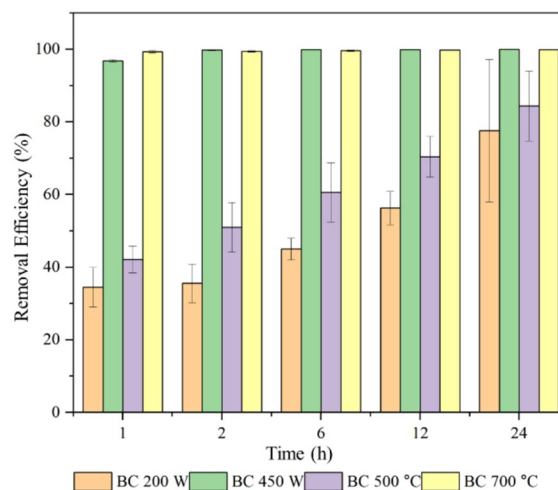
### 3.2.2 Effect of the initial Pb(II) concentration

Figure 4a and b show the effect of varying initial Pb(II) concentrations on the adsorption of BC 200 W (produced at  $238.4 \text{ }^\circ\text{C}$ ), BC 450 W (at  $475.1 \text{ }^\circ\text{C}$ ), BC 500  $^\circ\text{C}$ , and BC 700  $^\circ\text{C}$  using  $2 \text{ g L}^{-1}$  over a 24 h period. At a low concentration of  $5 \text{ mg L}^{-1}$ , the highest biochar removal efficiency ranged from BC 200 W > BC 500  $^\circ\text{C}$  > BC 700  $^\circ\text{C}$  > BC 450 W, where the removal efficiency ranged from 98.1 to 99.6%. At  $10 \text{ mg L}^{-1}$ , the removal efficiency changed slightly in the order of BC 450 W > BC 200 W > BC 500  $^\circ\text{C}$  > BC 700  $^\circ\text{C}$ , where the removal efficiency ranged from 89.6–98.6%. At  $20 \text{ mg L}^{-1}$ , all biochars removed heavy metals at a rate of 90% or more. However, a constant removal efficiency order was maintained from 50 to  $100 \text{ mg L}^{-1}$ , where the removal efficiency trend was observed to be BC 450 W > BC 700  $^\circ\text{C}$  > BC 500  $^\circ\text{C}$  > BC 200 W, and the removal efficiencies ranged between 38.4% and 96.7%. In all the trends observed at different initial Pb(II) concentration removal efficiencies, BC 450 W remained consistent with the high removal of Pb(II) [29]. This may be due to the biochar's high surface area, low pore size, and highly notable pores compared with those of the other biochars used in the analysis. It was further noted that at increased initial concentrations, the BC 500  $^\circ\text{C}$  and BC 700  $^\circ\text{C}$  removal efficiencies decreased because of the availability of sorption sites [31]. Statistical analyses were performed on the results and all p-values were observed to be insignificant (Table S2).

The adsorption capacities of BC at 200 W, BC 450 W, BC 500  $^\circ\text{C}$ , and BC 700  $^\circ\text{C}$  are consistent with the observed removal efficiencies. Notably, as the initial Pb(II) concentration increased, the adsorption capacity of the biochar increased [29]. Specifically, at  $20 \text{ mg L}^{-1}$ , all the biochars demonstrated similar adsorption capacities within the range of  $9.4$  to  $9.9 \text{ mg g}^{-1}$ . Overall, the highest adsorption capacity was achieved by BC 450 W, reaching  $31 \text{ mg g}^{-1}$  with a corresponding low removal efficiency of 63% at  $100 \text{ mg L}^{-1}$ . This suggested that adsorption saturation took place at high concentration of  $100 \text{ mg L}^{-1}$ , similar to findings observed by Cai and Ye [32]. Two isothermal models were employed to fit the adsorption data and determine the underlying factors contributing to this phenomenon.

### 3.2.3 Effect of contact time

To observe the effect of contact time, the experiment was conducted at a Pb(II) concentration of  $50 \text{ mg L}^{-1}$  because of the differences between conventional biochars and microwave biochars regarding the influence of the initial Pb(II) concentration. An adsorbent dosage of  $2 \text{ g L}^{-1}$  was applied, as per the findings of the effect of adsorbent dose, to investigate the effect of contact time. The results shown in Fig. 5 indicate that the adsorption of Pb(II) by BC 450 W and BC 700  $^\circ\text{C}$  consisted of two stages: (i) a very fast step at the beginning lasting from 0 to 1 h and (ii) a slow step lasting from 1 to 24 h, which depicted equilibrium being reached over this time, similar to findings by Chen et al. [30]. The maximum adsorption occurred within 24 h, with adsorption removal efficiencies of 99.9% and 99.8% for BC 450 W and BC 700  $^\circ\text{C}$ , respectively. This was possibly due to the large surface areas observed for the biochars (see Tables 4 and 5). However, the removal of Pb(II) using BC 200 W and BC 500  $^\circ\text{C}$  revealed lower removal efficiencies over the set period, resulting in lower removal efficiency compared to BC 450 W and BC 700  $^\circ\text{C}$ . This could be attributed to the surface area, pore volume, and accessibility of available adsorption sites [11, 31]. The biochars with lower pore volumes and surface areas (BC 200 W and BC 500  $^\circ\text{C}$ ) exhibited slower and lower adsorption over time owing to pore filling. Further investigation of the effect of time on the adsorption kinetics was performed. For BC 450 W and BC 700  $^\circ\text{C}$ , 1 h can be selected as the appropriate adsorption time; whereas for BC 200 W and BC 500  $^\circ\text{C}$ , time longer than 24 h may be required as pore volumes are lower and the availability of active sites on these biochars is less than those of BC 450 W and BC 700  $^\circ\text{C}$ .



**Fig. 5** Effect of time on the removal efficiency of Pb(II) using BC 200 W, BC 450 W, BC 500  $^\circ\text{C}$  and BC 700  $^\circ\text{C}$

**Table 4** Langmuir adsorption isotherm parameters for the adsorption of Pb(II) on BCs

Adsorbent	Isotherm Parameters					
	$K_L(\text{L mg}^{-1})$	$q_m(\text{mg g}^{-1})$	$R^2$	$R_L$	RMSE	$\chi^2$
BC 200 W	5.1	19	0.920	0.002	2.168	4.700
BC 450 W	0.4	79	0.994	0.026	1.531	2.343
BC 500 °C	0.2	79	0.995	0.058	1.269	1.609
BC 700 °C	0.1	89	0.978	0.061	2.705	7.317

**3.3 Adsorption isotherm models**

The associations between the adsorbates and adsorbents at different adsorbent doses, initial concentrations, and contact times were described using adsorption isotherms. Adsorption isotherms were used to clarify the metal adsorption mechanisms involved in the removal of Pb(II) in synthetic wastewater and the role of biochar in overall adsorption. The nonlinear Freundlich and Langmuir isotherm models were used in this study to examine the equilibrium adsorption data for Pb(II) removal.

The Langmuir isotherm model – Eq. (1) represents the nonlinear form of the Langmuir isotherm model:

$$q_e = \frac{q_m K_L C_e}{1 + K_L C_e} \tag{1}$$

where  $q_e$  is the amount of Pb(II) adsorbed ( $\text{mg g}^{-1}$ ) at equilibrium,  $q_m$  is the maximum monolayer adsorption capacity ( $\text{mg g}^{-1}$ ),  $C_e$  is the concentration of adsorbate at equilibrium ( $\text{mg L}^{-1}$ ), and  $K_L$  is the Langmuir constant ( $\text{L mg}^{-1}$ ).

The Freundlich isotherm is represented below by Eq. (2):

$$q_e = K_F C_e^{\frac{1}{n}} \tag{2}$$

where the Freundlich constant  $K_F$  ( $\text{L mg}^{-1}$ ) is a measure of the adsorption capacity, and  $n$  (dimensionless) indicates the adsorption effectiveness (where  $1/n \leq 1$  is effective and  $1/n \geq 1$  is ineffective).

The isotherm models were validated using root-square mean error (RSME) and chi-square ( $\chi^2$ ) tests

**Table 5** Freundlich adsorption isotherm parameters for the adsorption of Pb(II) on BCs

Adsorbent	Isotherm Parameters				
	$K_F(\text{L mg}^{-1})$	$1/n$	$R^2$	RSME	$\chi^2$
BC 200 W	8.9	0.17	0.860	2.794	7.804
BC 450 W	19.1	0.65	0.970	3.354	11.251
BC 500 °C	11.1	0.67	0.989	1.854	3.436
BC 700 °C	11.6	0.72	0.965	3.378	11.412

[33]. Additionally, a dimensionless parameter called the separation factor ( $R_L$ ) was calculated to express whether the isotherms are favorable ( $0 < R_L < 1$ ), linear ( $R_L = 1$ ), unfavorable ( $R_L > 1$ ) or irreversible ( $R_L = 0$ ). Equation (3) was used, and the results are displayed in Table 4.

$$R_L = \frac{1}{1 + K_L C_0} \tag{3}$$

By evaluating the important parameter values of the Freundlich and Langmuir isotherms in Tables 4 and 5, the Langmuir isotherm model proved to be the best fit model, in which the adsorbents displayed reasonable  $K_L$  values that show the affinity of the adsorbate to the adsorbent [26], good  $q_m$  values, low RSME, low  $\chi^2$  values, and good coefficient of determination ( $R^2$ ) ranging from 0.9808 to 0.9997; having  $q_m$  values ranging from 18 to 89  $\text{mg g}^{-1}$ , showing great adsorption capacities compared to most pristine plant-based biochar [34].  $R_L$  values that range from 0.002 to 0.061 indicate the favorable nature of the isotherms presented, where the lower values are more favorable because  $K_L$  has an inverse relation to  $R_L$ . The Langmuir adsorption isotherm is characterized by monolayer coverage on the surface of the biochars, indicating a homogenous distribution of Pb(II) on the active sites of the biochar [10, 14].

Although the Langmuir model fit the isotherm data of the adsorbate better than the Freundlich model, the Freundlich adsorption isotherm parameters were further evaluated. According to Islam et al. [26] and Shikuku and Mishra [33], lower values of  $1/n$  indicate strong interactions between the adsorbate and adsorbent. This can be seen in Table 5 for all the biochars, as the values are below 1.

Furthermore, according to Di et al. [34], a high  $K_F$  indicates greater adsorption capacity of the adsorbent of interest. The  $K_F$  values further validated the stronger interaction between the adsorbate and adsorbent, particularly for MAP-produced adsorbents, as biochar with the highest  $K_F$  value was BC 450 W, with a  $K_F$  value of 19.1  $\text{L mg}^{-1}$ . The Freundlich and Langmuir adsorption isotherm models are shown in Fig. 6a–d.

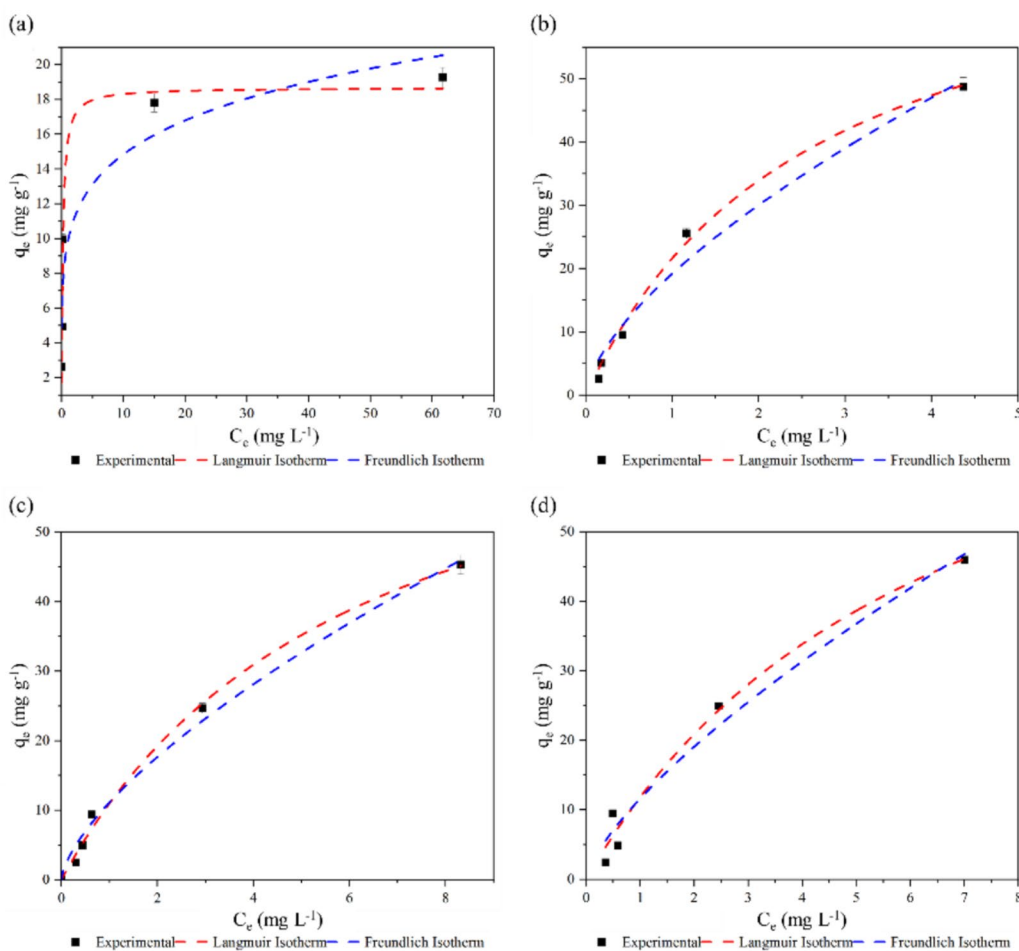


**Fig. 6** The Freundlich and Langmuir adsorption isotherms of **a**) BC 200 W, **b**) BC 450 W, **c**) BC 500 °C, and **d**) BC 700 °C for the adsorption of Pb(II) in 50  $\text{mg L}^{-1}$  solution at pH 5

### 3.4 Adsorption kinetics models

The rate of adsorption was investigated by employing both PFO and PSO kinetics models (Eqs. (4) and (5), respectively). The following equation was used to evaluate the pseudo-first-order model.

$$q_t = q_e(1 - e^{-k_1t}) \tag{4}$$

where  $q_t$  ( $\text{mg g}^{-1}$ ) is the adsorption amounts at time  $t$  (min) and  $k_1$  ( $\text{min}^{-1}$ ) is the PFO adsorption rate constant [35]. The following equation was used to evaluate the PSO model.

$$q_t = \frac{k_2q_e^2t}{1 + k_2q_e t} \tag{5}$$

where  $k_2$  is the PSO constant of PSO [35]. The kinetic models were validated using the RSME and  $R^2$ .

The adsorption behavior of lead ions (Pb(II)) on biochars produced at 200 W, 450 W, 500 °C, and 700 °C

aligns more accurately with the PSO kinetic model. Additionally, this is evidenced by the comparison of the correlation coefficients, where the PFO model yielded  $R^2$  values of 0.78 for BC 200 W and 0.91 for BC 500 °C. These figures are notably lower than those from the PSO, which are 0.87 and 0.96, respectively, indicating a better fit [33]. Moreover, the  $q_t$  values calculated using the PSO model were comparable to the Pb(II) adsorption experimental  $q_e$  values and did not fit well with the data obtained using the PFO model, as depicted in Table 6. However, for BC 450 W and BC 700 °C, the correlation coefficient was  $R^2=1.00$  for both PFO and PSO kinetic models. This may be due to the abundance and accessibility of binding sites on the biochar [35]. This indicates the occurrence of both chemisorption and physisorption processes, but to a greater extent, chemisorption as it has been found to be a rate-limiting step for the adsorption of lead onto biochar in previous studies [32]. The results obtained can be found in Table 6 and Fig. 7.

**Table 6** PFO and PSO kinetic parameters for Pb(II) adsorption from synthetic wastewater solution using selected biochar

Adsorbent	$q_e$ $\text{mg g}^{-1}$	Pseudo First Order (PFO)				Pseudo Second Order (PSO)			
		$q_t$ ( $\text{mg g}^{-1}$ )	RSME	$k_1$ ( $\text{min}^{-1}$ )	$R^2$	$q_t$ ( $\text{mg g}^{-1}$ )	RSME	$k_2$ ( $\text{g mg}^{-1} \text{min}^{-1}$ )	$R^2$
BC 200 W	19	16	3.03	0.01	0.78	18	2.32	0.00	0.87
BC 450 W	25	25	0.01	0.06	1.00	25	0.14	0.02	1.00
BC 500 °C	21	18	2.21	0.01	0.91	20	1.47	0.00	0.96
BC 700 °C	25	25	0.05	0.09	1.00	25	0.03	0.12	1.00

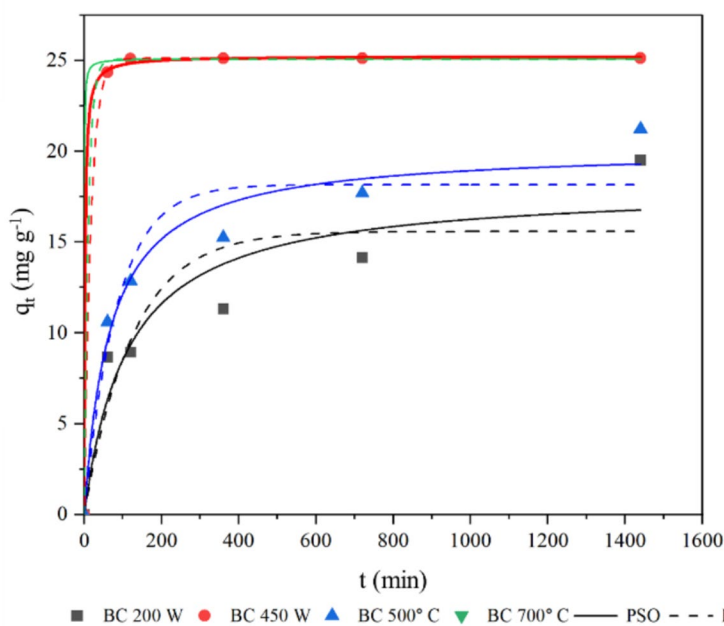


**Fig. 7** The research findings and the optimized PFO and PSO kinetic models for BC 200 W, BC 450 W, BC 500 °C, and BC 700 °C

CP is the most commonly reported method for producing biochar. While it offers benefits in terms of waste valorization, it also presents several challenges. These include uneven distribution of pyrolysis products due to non-selective heating, higher energy consumption, and longer times required to reach the target temperature [36]. Additionally, this method is often sluggish and inefficient, relying heavily on the instrument’s convection currents and the biomass’s thermal conductivity [20]. The low thermal conductivity of biomass further complicates achieving higher heat transfer rates, making the process time-consuming [23].

MAP stands out for its heating; at the level and uniform volume heating capability it offers. A distinguishing feature of this method. The process results in power conversion efficiency, and rapid yet thorough convection as its key advantages [11]. Additional perks reduced impurities in the end product, reduced thermal inertia effect and quick reaction times are advantages [20]. In summary,

MAP ensures controlled and efficient heating. Compared to pyrolysis methods for producing biochar, microwave irradiation results in levels of fixed carbon and significant lignin breakdown. It also enhances carbon stability. Increases both surface area and pore volume. The quick heating process in microwave pyrolysis fosters the formation of structures, oxygen functional groups on surfaces and catalytic properties [23]. Microwave derived biochar exhibits consistent chemical characteristics. Unlike conventional approaches; MAP uniformly heats a sample from within allowing for thorough biomass pyrolysis before application as biochar [37].

With this, this distinctly shows the capability of MAP being more scientifically feasible and economically viable for the production of biochar, especially when considering production time, the principles behind the method used and the quality of the biochar produced through physicochemical analyses. The results obtained in this study further prove that biochar produced at 450 W was

more effective in adsorbing Pb(II) when observing the adsorption isotherms and kinetic studies conducted.

### 3.5 Possible adsorption mechanism analysis

A variety of reactions occur between an adsorbate and an adsorbent, which helps to determine the type of mechanisms that occur during investigation. These reactions include chemisorption and physisorption reactions [3, 38]. Considering that the Langmuir model was the best model for Pb(II) adsorption onto the biochars, monolayer chemisorption which entails pore filling, surface complexation, electrostatic interaction of Pb(II) most likely occurred on the homogenous surface area of the investigated biochar [3]. Furthermore, since the PSO model best describes the adsorption kinetics of the study, it can be noted that, similar to Shafiq et al. [29], the adsorption kinetic model adheres more to the chemisorption mechanism. To identify the forms of the chemisorption mechanism in this study, FTIR was further investigated and compared with the initial FTIR (Fig. 2a and b).

To further understand the adsorption mechanism of Pb(II) on the BC surface, FTIR spectral analyses of the BC 200 W, BC 450 W, BC 500 °C, and BC 700 °C adsorbents after Pb(II) adsorption are shown in Fig. 8a and b. Sharp new bands were observed at approximately 1630  $\text{cm}^{-1}$ , where a decreased shift in the spectra occurred because Pb(II) was actively complexed with the carboxylic acid group initially observed in the biochars before adsorption (approximately 1700  $\text{cm}^{-1}$ , see Fig. 2a and b), an indication of surface complexation between the carboxylic acid group and the metal ion Pb(II) similar to findings by Aborisade et al. [39].

Narrower peaks were also observed at approximately 1380  $\text{cm}^{-1}$ , which are characteristic of a shift in the spectra observed at 1600  $\text{cm}^{-1}$  before adsorption. The adsorption of Pb(II) resulted in a shift in the spectra, indicating a compound with weak C-H bending bands (alkane) and showing the hydrophilic characteristics of the biochars [11, 29]. The shift in the identified bands belong to the alkene (C=C) group, demonstrating that Pb(II) diffuses onto the selected BC biochar to fill the biochar pores, which is a physical process (Fig. 8) on the biochar surface [3, 29, 31]. This is also verified by the adsorption kinetic models, whereby although the best fit model was the PSO model, the PFO (particularly at higher temperatures and power) displayed good  $q_t$  values and good coefficient correlation values, indicating that physical processes exist in the adsorption of Pb(II). Other previously observed functional groups (O-H and C-O) remained constant; however, asymmetric C-H stretching vibrations at approximately 2900  $\text{cm}^{-1}$  were no longer observed in the biochars generated through conventional pyrolysis, indicating a decreased “nonpolar aliphatic fraction”, as stated by Aborisade et al. [3]. Electrostatic interactions may have occurred on the surface of biochar due biochar produced from plant-based material exhibiting negative charges which is depicted by zeta potential observed in the Fig. S3. Similarly, the findings observed are closely related with those found by Zhou et al. [28]. Possible mechanisms are depicted in Fig. 9.

### 3.6 Comparison to other adsorbents for Pb(II) adsorption

The study conducted shows similar adsorption capacities among the biochar experimented upon over a period of 24 h, with slight differences observed where biochar

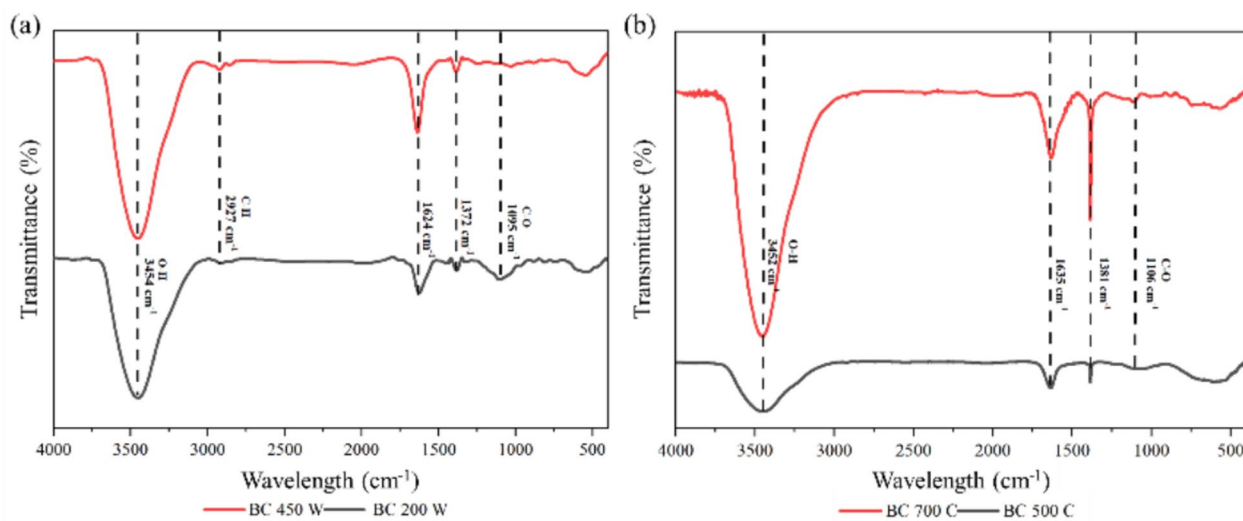


**Fig. 8** FTIR spectra of **a**) microwave pyrolyzed and **b**) conventional pyrolyzed bamboo chopstick biochar after the adsorption of Pb(II)

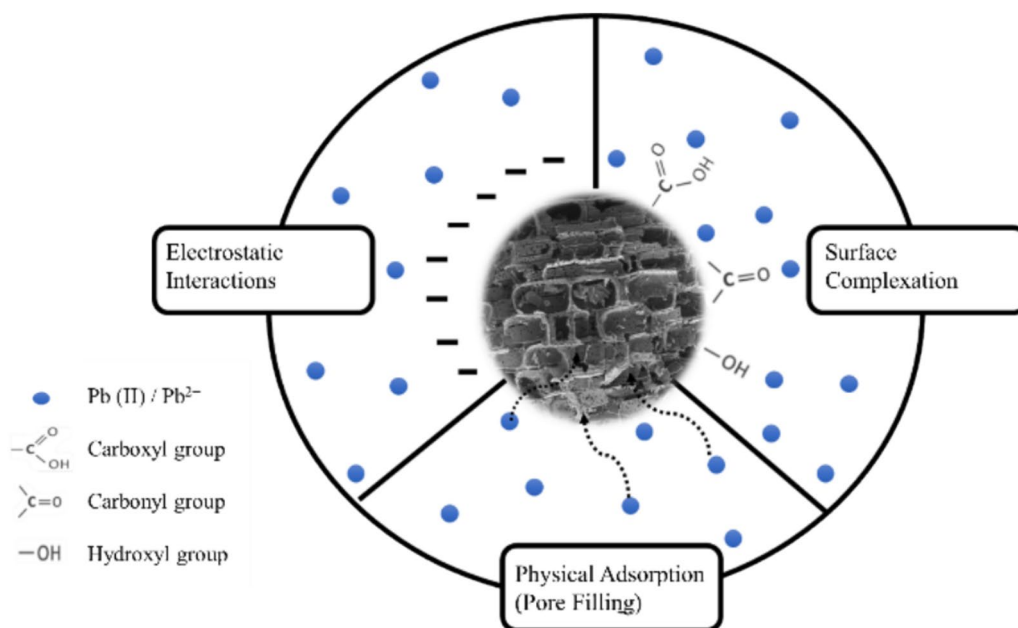


**Fig. 9** Depiction of the possible mechanisms on the different BCs for Pb(II) adsorption

produced at 450 W produced a higher adsorption capacity compared to the other biochar of interest. Studies conducted by Shi et al. [36] further confirm that low adsorption capacities can be attained in Pb(II) adsorption using CP, which is also influenced by the adsorbent dose and the initial concentrations used in the study. However, when biochar produced by CP is modified, greater adsorption capacities are observed. This is primarily due to more functional groups introduced onto the surface of the modified biochar, giving the biochar a greater chance at adsorption. However, according to Potnuri et al. [19], biochar produced using MAP exhibit greater surface area compared to CP. This is highly observed on biochar demonstrated on Table 7 where Nzediegwu et al. [7] and Qi et al. [37] use pristine biochar and further show similar or higher adsorption capacities of Pb(II) than those of modified CP-produced biochar. In some instances, biochar may not necessarily need to be modified but modification may improve the rate of adsorption and removal efficiency as well (Table 7).

### 3.7 Limitations of the study

This study found that comparing biochar generated by various processes (MAP and CP) at variable but comparable temperatures provided comparable characteristics but differing overall outcomes in the adsorption and removal of Pb(II) in synthetic wastewater. However, it was discovered that significant limitations to the study should be acknowledged. First, consider the temperature differences between the two ways for producing biochar.

This is because the operator controls the CP temperature, whereas operator merely controls the MAP power and the thermocouple monitors the temperature. Secondly, the impact of the biochar generated might not apply to other heavy metals present in heavy metal wastewater. The use of single-element synthetic wastewater could have been the limiting factor in this section, preventing a thorough analysis with other heavy metals present and limiting the comparison of Pb(II) elimination with other metals in solution. To determine how well biochar works to remove additional heavy metals from aqueous media, more research is needed. Thirdly, the study should be optimized by factoring various aspects using the design of experiment to ensure that time, resources, and accuracy are taken into account before fully experimenting without taking into account crucial factors like time, temperature, initial concentration, pH, and contact time. This is currently being implemented in on-going studies.

With these drawbacks, the study's encouraging findings highlight the potential benefits of MAP biochar over CP-produced biochar and the ways in which it may be used to remove pollutants from solutions. Aspects such as evaluating and comparing the cost-effectiveness in using the pyrolytic methods investigated will assist in investigating the financial implications associated with the potential real-world application of the biochar being produced, optimization of studies considering a range of parameters using design of experiments, and the effects of the modification of the most feasible biochar is yet to be investigated too.

**Table 7** Comparison of the adsorption capacities of biochar produced using MAP and CP

Precursor Material	Method	Temperature (°C)/ Power (W)	Modified/ Pristine	Metal(s) Removed	Adsorbent Dose	q <sub>e</sub> (mg g <sup>-1</sup> )	References	
Bamboo Chopsticks	Microwave-Assisted Pyrolysis	200 W	Pristine	Pb (II)	2 g L <sup>-1</sup>	18	This study	
		450 W				24		
	Conventional pyrolysis (Tube furnace)	500 °C	Pristine	23				
Empty Fruit Bunch (EFBB)	Conventional Pyrolysis	700 °C	Course-EFBB Medium-EFBB Fine-EFBB	Pb(II)	2.5 g L <sup>-1</sup>	23	[25]	
		250 °C				55		
						58		
<i>Eupatorium adenop-horum</i>	Conventional Pyrolysis (Tube furnace)	800 °C	Modified CEA-1	Pb(II)	0.5 g L <sup>-1</sup>	18	[40]	
			Modified CEA-2			98		
			Modified CEA-3			84		
Canola ( <i>Brassica napus</i> ) Manure Pellet	Microwave assisted pyrolysis	500 °C	Pristine	Pb(II)	1 g L <sup>-1</sup>	106	[7]	
						Saw dust of white spruce ( <i>Picea glauca</i> )		60
						Wheat ( <i>Triticum aestivum</i> )		7
Hemp	Microwave assisted pyrolysis	600 °C, 2.7 kW	Magnetically Modified	Pb (II)	0.5 g L <sup>-1</sup>	61	[33]	
			Unmodified/ Pristine			27		

**4 Conclusion**

MAP and CP have proven effective in producing biochar from waste BC and in removing Pb(II) from synthetic wastewater. The characteristics of the biochar investigated, particularly SEM, BET, elemental analyses, and FTIR, were able to provide a foundation that could clarify the effectiveness and possible changes in the biochar applied in the study after adsorption. The biochars produced using MAP provided adsorbents comparable to those produced by CP. The surface areas (S<sub>BET</sub>) were comparable, although BC 450 W (produced at approximately 475 °C) had a larger surface area and slightly smaller pores than BC 700 °C. The surface morphology obtained using SEM revealed a honeycomb yet tubular structure, where a difference was observed between the microwave-assisted biochar, which produced biochar with highly visible pores, and the biochar produced using CP, where the structure displayed a few pores. FTIR was used for chemical characterization of the biochar produced, and the results were similar for both pyrolytic methods used before application. The efficiency of biochar in removing Pb(II) was evaluated through various pyrolysis techniques and temperatures, taking into account factors such as the amount of adsorbent, the initial concentration of Pb(II), and the duration of contact. The ability of biochar to adsorb was found to be stable and correlated with the initial concentration utilized. Following the batch adsorption experiments, the Langmuir

and Freundlich isotherms were both examined. The Langmuir isotherm was identified as the most accurate model. Additionally, the PSO kinetic model was recognized as the most suitable kinetic model, highlighting the chemical nature of Pb(II) adsorption across all biochar samples tested in this research. The FTIR results showed that the biochar surface functional groups, carboxylic and aromatic carbons, were involved in Pb(II) adsorption. Furthermore, the shift in these functional groups after adsorption suggested that surface complexation was the primary adsorption mechanism. Generally, a BC concentration of 50 mg L<sup>-1</sup> appears to be more suitable for Pb(II) removal in synthetic wastewater based on the biochar characteristics, the effects of adsorbent dosage, the effects of initial concentration and contact time, and the obtained adsorption isotherm and kinetic results. Overall, BC biochar was found to be a highly effective and environmentally friendly solution for tackling the issue of Pb(II) polluted water and managing the excess amount of chopstick waste. In contributing to the already existing knowledge where biochar is used primarily for characterization and in soil remediation, narrowly addressing pollution in the form of Pb in wastewater using BC biochar produced using CP and MAP, and comparatively discussing the findings is distinctly novel. Future work including design optimization studies would be best to use going forward, fieldwork implementation, and possibly evaluating the cost–benefit analysis of using both methods implemented in this study for largescale production.

## Supplementary Information

The online version contains supplementary material available at <https://doi.org/10.1186/s42834-024-00238-6>.

Supplementary Material 1.

### Acknowledgements

The authors express their gratitude to National Taiwan University (NTUCCP-111L901003, NTU-111L8807, NTU-111L895104, and NTU-112L893904), the Ministry of Education (MOE) in Taiwan, and the Ministry of Science and Technology (MOST) in Taiwan (MOST111-2621-M-002-012 and MOST112-2221-E-002-068) for their financial support. The perspectives presented in this publication are solely those of the authors and do not reflect the official views of the aforementioned institutions.

### Authors' contributions

Thembeke Mabaso and Professor Shang-Lien Lo contributed to the conception and design of the study and further reviewed and edited the manuscript. The material preparation, data analysis, and original manuscript drafting were performed by Thembeke Mabaso. Professor Pei-Te Chiueh and Thembeke Mabaso conducted the research investigations and data collection. Corresponding author Professor Shang-Lien Lo is the responsible supervisor and funding acquirer. All the authors have read and approved the final manuscript.

### Funding

This work was financially supported by National Taiwan University (NTUCCP-111L901003, NTU-111L8807, NTU-111L895104, and NTU-112L893904), the NTU Research Center for Future Earth from The Featured Areas Research Center Program within the framework of the Higher Education Sprout Project by the Ministry of Education (MOE) in Taiwan, and the Ministry of Science and Technology in Taiwan (MOST111-2621-M-002-012 and MOST112-2221-E-002-068).

### Data availability

Data will be made available upon request.

### Declarations

### Competing interests

The authors declare that they have no competing interests.

Received: 28 May 2024 Accepted: 3 December 2024

Published online: 18 December 2024

### References

- Ren J, Zheng L, Su Y, Meng P, Zhou Q, Zeng H, et al. Competitive adsorption of Cd(II), Pb(II) and Cu(II) ions from acid mine drainage with zero-valent iron/phosphoric titanium dioxide: XPS qualitative analyses and DFT quantitative calculations. *Chem Eng J*. 2022;445:136778.
- Gupta S, Sireesha S, Sreedhar I, Patel CM, Anitha KL. Latest trends in heavy metal removal from wastewater by biochar based sorbents. *J Water Process Eng*. 2020;38:101561.
- Aborisade MA, Oba BT, Kumar A, Liu J, Chen D, Okimiji OP, et al. Remediation of metal toxicity and alleviation of toxic metals-induced oxidative stress in *Brassica chinensis* L using biochar-iron nanocomposites. *Plant Soil*. 2023;493:629–45.
- Garcia-Valero A, Martinez-Martinez S, Faz A, Rivera J, Acosta JA. Environmentally sustainable acid mine drainage remediation: Use of natural alkaline material. *J Water Process Eng*. 2020;33:101064.
- Aborisade MA, Feng A, Oba BT, Kumar A, Battamo AY, Huang M, et al. Pyrolytic synthesis and performance efficacy comparison of biochar-supported nanoscale zero-valent iron on soil polluted with toxic metals. *Arch Agron Soil Sci*. 2023;69:2249–66.
- Al-Zoubi H, Rieger A, Steinberger P, Pelz W, Haseneder R, Härtel G. Nanofiltration of Acid Mine Drainage. *Desalin Water Treat*. 2010;21:148–61.
- Nzediegwu C, Naeth MA, Chang SX. Lead(II) adsorption on microwave-pyrolyzed biochars and hydrochars depends on feedstock type and production temperature. *J Hazard Mater*. 2021;412:125255.
- Bacirhonde PM, Dzade NY, Eya HI, Kim CS, Park CH. A potential peanut shell feedstock pyrolyzed biochar and iron-modified peanut shell biochars for heavy metal fixation in acid mine drainage. *ACS Earth Space Chem*. 2022;6:2651–65.
- Qin J, Wang X, Deng M, Li H, Lin C. Red mud-biochar composites (co-pyrolyzed red mud-plant materials): Characteristics and improved efficacy on the treatment of acidic mine water and trace element-contaminated soils. *Sci Total Environ*. 2022;844:157062.
- Nqombolo A, Mpupa A, Gugushe AS, Moutloali RM, Nomngongo PN. Adsorptive removal of lead from acid mine drainage using cobalt-methylimidazole framework as an adsorbent: kinetics, isotherm, and regeneration. *Environ Sci Pollut R*. 2019;26:3330–9.
- Lam SS, Azwar E, Peng W, Tsang YF, Ma NL, Liu Z, et al. Cleaner conversion of bamboo into carbon fibre with favourable physicochemical and capacitive properties via microwave pyrolysis combining with solvent extraction and chemical impregnation. *J Clean Prod*. 2019;236:117692.
- Shirvanimoghaddam K, Czech B, Abdikhebari S, Brodie G, Kończak M, Krzyszcak A, et al. Microwave synthesis of biochar for environmental applications. *J Anal Appl Pyrol*. 2022;161:105415.
- Phadungbut P, Koo-amornpattana W, Bumroongsri P, Ratchahat S, Kunthakudee N, Jonglertjunya W, et al. Adsorptive purification of CO<sub>2</sub>/H<sub>2</sub> gas mixtures of spent disposable wooden chopstick-derived activated carbon: Optimal synthesis condition. *Sep Purif Technol*. 2022;291:120948.
- Stylianou M, Christou A, Dalias P, Polycarpou P, Michael C, Agapiou A, et al. Physicochemical and structural characterization of biochar derived from the pyrolysis of biosolids, cattle manure and spent coffee grounds. *J Energy Inst*. 2020;93:2063–73.
- Wijitkosum S. Repurposing disposable bamboo chopsticks waste as biochar for agronomical application. *Energies*. 2023;16:771.
- Chaturvedi K, Singhwani A, Dhargar M, Mili M, Gorhae N, Naik A, et al. Bamboo for producing charcoal and biochar for versatile applications. *Biomass Convers Bior*. 2024;14:15159–85.
- Xu R, Deng S, Wang W, Schenk J, Wang F. Structural features and combustion behaviour of waste bamboo chopstick chars pyrolysed at different temperatures. *Bioenerg Res*. 2020;13:439–51.
- Mujtaba M, Fernandes Fraceto L, Fazeli M, Mukherjee S, Savassa SM, Araujo de Medeiros G, et al. Lignocellulosic biomass from agricultural waste to the circular economy: a review with focus on biofuels, biocomposites and bioplastics. *J Clean Prod*. 2023;402:136815.
- Potnuri R, Surya DV, Rao CS, Yadav A, Sridevi V, Remya N. A review on analysis of biochar produced from microwave-assisted pyrolysis of agricultural waste biomass. *J Anal Appl Pyrol*. 2023;173:106094.
- Godwin PM, Pan Y, Xiao H, Afzal MT. Progress in preparation and application of modified biochar for improving heavy metal ion removal from wastewater. *J Bioresour Bioprod*. 2019;4:31–42.
- Chang CC, Chen CP, Yang CS, Chen YH, Huang M, Chang CY, et al. Conversion of waste bamboo chopsticks to bio-oil via catalytic hydrothermal liquefaction using K<sub>2</sub>CO<sub>3</sub>. *Sustain Environ Res*. 2016;26:262–7.
- Huang YF, Chiueh PT, Lo SL. Carbon capture of biochar produced by microwave co-pyrolysis: adsorption capacity, kinetics, and benefits. *Environ Sci Pollut R*. 2023;30:22211–21.
- Mukome FND, Zhang X, Silva LCR, Six J, Parikh SJ. Use of chemical and physical characteristics to investigate trends in biochar feedstocks. *J Agr Food Chem*. 2013;61:2196–204.
- Roy S, Kumar U, Bhattacharyya P. Synthesis and characterization of exfoliated biochar from four agricultural feedstock. *Environ Sci Pollut R*. 2019;26:7272–6.
- Fahmi AH, Samsuri AW, Jol H, Singh D. Physical modification of biochar to expose the inner pores and their functional groups to enhance lead adsorption. *RSC Adv*. 2018;8:38270–80.
- Islam MS, Kwak JH, Nzediegwu C, Wang S, Palansuriya K, Kwon EE, et al. Biochar heavy metal removal in aqueous solution depends on feedstock type and pyrolysis purging gas. *Environ Pollut*. 2021;281:117094.
- Mari Selvam S, Balasubramanian P. Influence of biomass composition and microwave pyrolysis conditions on biochar yield and its properties: a machine learning approach. *Bioenerg Res*. 2023;16:138–50.

28. Zhou N, Zu J, Feng Q, Chen H, Li J, Zhong ME, et al. Effect of pyrolysis condition on the adsorption mechanism of heavy metals on tobacco stem biochar in competitive mode. *Environ Sci Pollut R*. 2019;26:26947–62.
29. Shafiq M, Alazba AA, Amin MT. Kinetic and isotherm studies of Ni<sup>2+</sup> and Pb<sup>2+</sup> adsorption from synthetic wastewater Using *Eucalyptus camdulis*—derived biochar. *Sustainability*. 2021;13:3785.
30. Chen L, Hu J, Wang H, He Y, Deng Q, Wu F. Predicting Cd(II) adsorption capacity of biochar materials using typical machine learning models for effective remediation of aquatic environments. *Sci Total Environ*. 2024;944:173955.
31. Liu S, Peng S, Zhang B, Xue B, Yang Z, Wang S, et al. Effects of biochar pyrolysis temperature on thermal properties of polyethylene glycol/biochar composites as shape-stable biocomposite phase change materials. *RSC Adv*. 2022;12:9587–98.
32. Cai G, Ye ZL. Concentration-dependent adsorption behaviors and mechanisms for ammonium and phosphate removal by optimized Mg-impregnated biochar. *J Clean Prod*. 2022;349:131453.
33. Shikuku VO, Mishra T. Adsorption isotherm modeling for methylene blue removal onto magnetic kaolinite clay: a comparison of two-parameter isotherms. *Appl Water Sci*. 2021;11:103.
34. Di J, Ruan Z, Zhang S, Dong Y, Fu S, Li H, et al. Adsorption behaviors and mechanisms of Cu<sup>2+</sup>, Zn<sup>2+</sup> and Pb<sup>2+</sup> by magnetically modified lignite. *Sci Rep*. 2022;12:1394.
35. Simonin JP. On the comparison of pseudo-first order and pseudo-second order rate laws in the modeling of adsorption kinetics. *Chem Eng J*. 2016;300:254–63.
36. Shi J, Fan X, Tsang DCW, Wang F, Shen Z, Hou D, et al. Removal of lead by rice husk biochars produced at different temperatures and implications for their environmental utilizations. *Chemosphere*. 2019;235:825–31.
37. Qi G, Pan Z, Zhang X, Chang S, Wang H, Wang M, et al. Microwave biochar produced with activated carbon catalyst: Characterization and adsorption of heavy metals. *Environ Res*. 2023;216:114732.
38. Liu C, Lin J, Chen H, Wang W, Yang Y. Comparative study of biochar modified with different functional groups for efficient removal of Pb(II) and Ni(II). *Int J Env Res Pub He*. 2022;19:11163.
39. Aborisade MA, Feng A, Zheng X, Oba BT, Kumar A, Battamo AY, et al. Carbothermal reduction synthesis of eggshell-biochar modified with nanoscale zerovalent iron/activated carbon for remediation of soil polluted with lead and cadmium. *Environ Nanotechnol Monit Manag*. 2022;18:100726.
40. Liu, D, Hao, Z, Chen, D, Jiang, L, Li, T, Tian, B, et al. Use of Eggshell-Catalyzed Biochar Adsorbents for Pb Removal from Aqueous Solution. *ACS Omega*. 2022;7:21808–19.

## Publisher's Note

Springer Nature remains neutral with regard to jurisdictional claims in published maps and institutional affiliations.